Maximum Likelihood reconstruction for fluorescence Optical Projection Tomography

A. Darrell, H. Meyer, U. Birk, K. Marias, *Member, IEEE,* M. Brady, *Senior Member, IEEE* and J. Ripoll.

***Abstract* - Tomographic reconstruction of fluorescence Optical Projection Tomography (OPT) data is usually performed using the standard Filtered Back Projection (FBP) algorithm. However, there are several physical aspects of fluorescence OPT that pose major challenges for the FBP algorithm. These include blurring, and the fact that for an isotropically emitting point source (or fluorophore), the power received by an objective aperture decreases with the inverse square of the distance to the source. These two effects are shown to result in *qualitative* and *quantitative* inaccuracies in fluorescence OPT reconstructions obtained using standard FBP. A model of image formation is developed which includes the effects of isotropic emission and blurring. The model is used to calculate a probabilistic system matrix for use in the Maximum Likelihood Expectation Maximisation algorithm, which leads to reconstructions that are both *qualitatively* superior and *quantitatively* correct.**

***Index Terms*— Optical Projection Tomography, Iterative Image Reconstruction, Maximum likelihood expectation maximisation, fluorescence.**

I. INTRODUCTION

Optical Projection Tomography is a relatively new imaging modality that can be used to obtain three dimensional images both of absorption and fluorescence in biological samples on the micron to centimeter range [1]. Reported applications include organ inter-relationship studies in mice [2], three dimensional imaging and quantification within rodent organs [3], modeling of early human brain development [4], visualising plant development and gene expression [5], three dimensional imaging of isolated cell nuclei [6], 3D imaging of Xenograft tumours [7], cell tracing [8], three dimensional imaging of Drosophila melanogaster [9], spatio-temporal analysis of the Zebrafish [10,11], developmental embryology and gene expression [1,12,13], in-vitro 4D quantification of growing mouse limb buds [14], three-dimensional tissue organization and gene expression in arabidopsis [15], gene expression in the adult mouse brain [16] and gene expression in the foregut and lung buds in humans [17].

Arguably, all applications of fluorescence OPT would benefit from *qualitatively* superior reconstructions. In addition, applications where quantitative results are required would benefit from *quantitatively* correct reconstructions; i.e. reconstructions in which, say, the intensities of two areas of gene expression could be reliably compared in light of the knowledge that two equal intensity groups of fluorophores in the sample give rise to two equal intensity groups of fluorophores in the reconstruction.

The depth of field (DOF) of an imaging system is a spatial region in which objects appear reasonably well focused in images. The focal plane of an imaging system can be found at the midpoint of its DOF. Most OPT setups incorporate an iris either built into or positioned behind the objective. An iris positioned in this way can be used to adjust the depth of field of the imaging system so as to strike a balance between a high signal to noise ratio and minimal blurring. However, in all cases there is at least some blurring present.

The *qualitative* effects of blurring in OPT have been reported, and efforts have been made to deal with this issue both by refining image forming optics [18] and by pre-processing projections to remove blur prior to the use of the FBP algorithm [19]. In [18] the authors propose using a pinhole to reduce blurring in an OPT setup. While the pinhole approach goes some way to reducing blur, it leads to other difficulties, such as a significant reduction in signal to noise ratio. In addition, the pin hole approach does nothing to counter the effects of the inverse square law, which has a *quantitative* effect on FBP reconstructions. A pre-processing based method of

Manuscript received July 5th, 2008. This work was supported by E.U. Integrated Project "Molecular Imaging" LSHG-CT-2003-503259. A. Darrell and H. Meyer acknowledge support from EST Molec-Imag MEST-CT-2004-007643. U. Birk acknowledges support from Marie-Curie Intra-European Fellowship MEIF-CT-2006-041827.

A. Darrell is with ICS-FORTH, Vassilika Vouton, P.O.Box 1385, GR 711 10 Heraklion, Greece and Department of Engineering Science, Oxford University, Parks Road, Oxford OX1 3PJ and (email: adarrell@ics.forth.gr).

K. Marias was with Medical Vision Laboratory, Department of Engineering Science, Oxford University, Parks Road, Oxford OX1 3PJ. He is now with the ICS-FORTH, Vassilika Vouton, P.O.Box 1385, GR 711 10 Heraklion, Greece (email: kmarias@ics.forth.gr).

J. Ripoll, H. Meyer and U. Birk are with IESL-FORTH, Vassilika Vouton, P.O.Box 1385, GR 711 10 Heraklion, Greece (email: {jripoll, heimeyer}@iesl.forth.gr and uspoeri@kip.uni-heidelberg.de)

M. Brady is with Medical Vision Laboratory, Department of Engineering Science, Oxford University, Parks Road, Oxford OX1 3PJ, UK. (email: jmb@robots.ox.ac.uk).

reducing blur in a slightly different OPT set-up is described in [19]. The set-up described in [19] requires that samples are positioned slightly off the focal plane so that only half of the sample is in reasonable focus. The highly out of focus light received from the other half of the sample is then de-emphasized. This method is not applicable to the setup described in this paper because samples are positioned so that the centre of rotation lies at the focal plane thereby achieving symmetrical focus of the sample.

In a recent paper [20], we identified the *quantitative* effects of blur and isotropic emission in fluorescence OPT. We proposed a modification to the FBP algorithm which enables *quantitatively* correct reconstructions to be obtained, despite blurring.

In this paper, we present a method of accounting for both the *qualitative* and the *quantitative* effects of isotropic emission and blurring in fluorescence OPT reconstruction.

II. METHODS

A. Experimental Setup

The OPT system used in the experiments reported in this paper consists of various components. Several infinity corrected microscope lenses *[Infinity, USA and Mitutoyo, USA]* are available for use with a custom filter holder for housing optical filters suitable for imaging various fluorescent proteins. An iris is incorporated into the design which allows the depth of field of the system to be adjusted. These parts are joined to an infinity corrected mono microscope tube *[Infinity, USA]* which is in turn mounted to an iXon ICCD *[Andor, Northern Ireland]*.

Samples are mounted onto a rotation stage *[Standa, Lithuania]* with x-y adjustment so as to be able to position samples close to the centre of rotation, thereby minimising sample precession.

To reduce reflections, samples are immersed in an 86% glycerol solution with a refractive index of 1.4535 *[Merck, Germany]* within the lower end of the capillary tube. The lower end of the capillary tube is itself immersed in the same brand of index matching fluid contained within a custom designed chamber with glass windows which allow excitation and fluorescence to enter and exit respectively. The refraction between the surface of a sample and the surrounding glycerol solution within the capillary tube is not presently accounted for; nor is the refraction between the flat surface of the chamber and the air.

The system is controlled using custom LabView software developed at IESL, FORTH.

B. Measurement of the system impulse response and depth of field

Using a 2.5x objective and a typical iris setting for fluorescence OPT imaging with this objective, a sequence of fluorescence OPT images of a sub-resolution $۳.۱\mu m$ diameter green fluorescent microsphere [*Duke Scientific, USA*] were obtained for 200 equidistant positions along the optical axis of the OPT system.

While the DOF as defined by constant Full Width at Half Maximum (FWHM) appears to be around 400 μm , it can be seen that the maximum intensity in images within that depth of field changes by as much as 80%, which suggests that raw fluorescence OPT projections may not lead to *quantitatively* correct reconstructions unless some account of the physics of blur is made within the reconstruction algorithm.

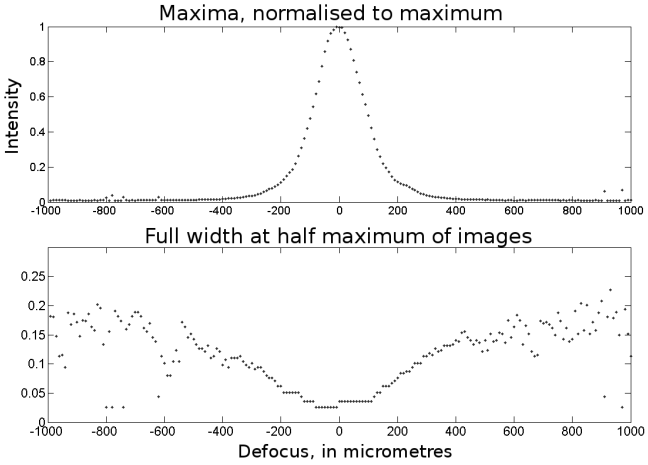

Figure 1. Top: Maximum values plotted against defocus for images of a microsphere at 200 equidistant positions ranging from around -1000µm to +1000µm defocus. Bottom: The FWHM of the same images plotted against defocus. Over a DOF ranging from around -200µm to 200µm, the indicative intensity varies by as much as 80% of its maximum value.

C. Phantom experiment

An OPT phantom was prepared which consisted of several $۳.۱\mu m$ diameter green fluorescent microspheres [*Duke Scientific, USA*] embedded in an indexed matched agarose gel. The gel/microsphere solution was allowed to set within the same type of capillary tube used for normal OPT experiments. 500 fluorescence OPT projections of the sample were taken over a range of 2π radians. Despite the microspheres all having approximately the same intensity, the standard FBP algorithm assigned a radial distance dependent intensity to microspheres, as shown in figure 2.

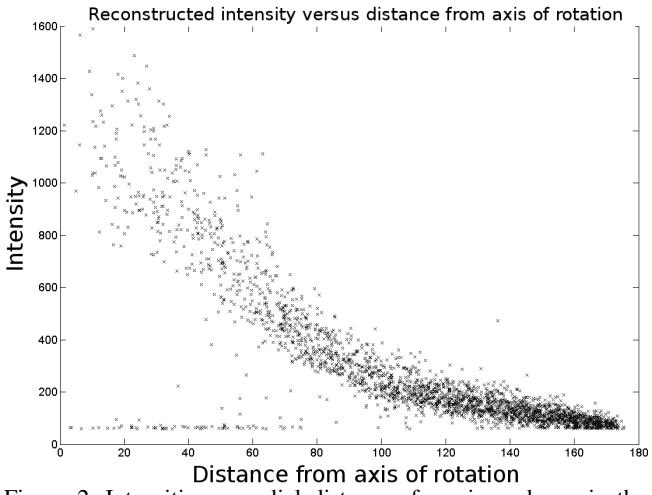

Figure 2. Intensities vs radial distances for microspheres in the FBP reconstruction of a microsphere based phantom. This plot shows a marked reduction in the intensity assigned by the FBP algorithm, from 1600 near the centre of the sample down to around 60 near the edges.

In addition to assigning reduced intensities towards the edges of reconstructions, the FBP algorithm also results in lower resolution and streak artifacts in these areas. See figure 3.

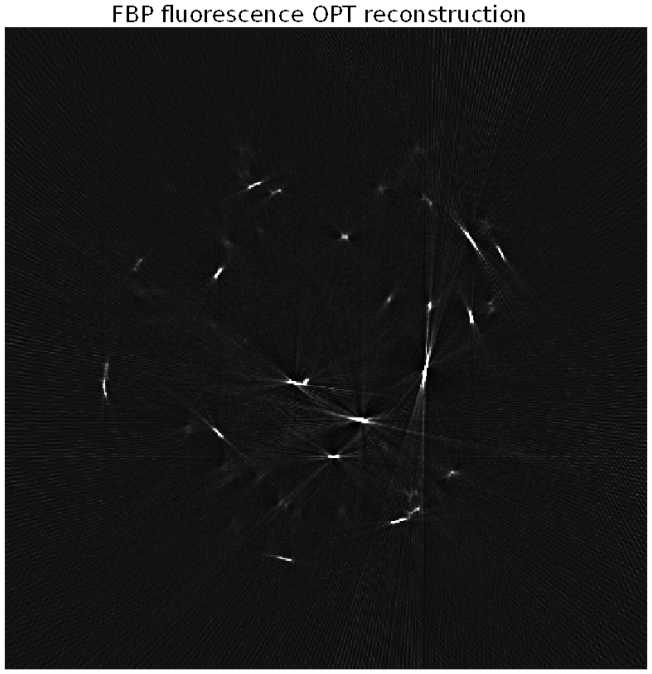

Figure 3. One image from a stack of reconstructed images of the microsphere phantom obtained using FBP. The microspheres are less well resolved towards the edge of the image.

D. Maximum Likelihood reconstruction

Maximum likelihood reconstruction for Positron Emission Tomography (PET) was introduced by Shepp and Vardi in 1982 [21]. In their paper, they fully discuss the Maximum Likelihood Expectation Maximisation algorithm. A brief recap of that discussion is given here.

1) The ML-EM algorithm

Consider a discrete spatial domain $\mathbf{f}$ of N elements which fully encompasses the DOF of the imaging system and the sample being imaged. Suppose that a model $\mathbf{H}$ of the imaging system exists such that the full set of projections $\mathbf{g}$ are given by the relation

$$\mathbf{g}=\mathbf{H}\mathbf{f} \qquad 1$$

where the i^{th} CCD detector pixel value is given by

$$g_i=h_i f, \quad i=1,\ldots,P \qquad 2$$

and P is the total number of CCD pixel values recorded in all projections. It is important to note that P is not the number of projections, but the number of projections multiplied by the number of CCD pixels on the CCD detector.

The ML-EM algorithm is an iterative algorithm which starts with an initial estimate $\hat{\mathbf{f}}^{(0)}$ of the body and iteratively computes successive improved estimates $\hat{\mathbf{f}}^{(\mathrm{n})}$. The algorithm consists of the repetition of two key steps which are known as the expectation and maximisation steps.

The expectation step:
Given the current estimate $\hat{\mathbf{f}}^{(\mathrm{n})}$, find

$$Q(\mathbf{f}|\hat{\mathbf{f}}^{(\mathrm{n})})=E[\ln \mathrm{p}(\mathbf{s}|\mathbf{f})|\mathbf{g},\hat{\mathbf{f}}^{(\mathrm{n})}]$$

The maximisation step:
Set $\hat{\mathbf{f}}^{(\mathrm{n}+1)}=\mathbf{f}$, where $\mathbf{f}$ maximises $Q(\mathbf{f}|\hat{\mathbf{f}}^{(\mathrm{n})})$.

Derivations of the expectation and maximisation steps for emission tomography can be found in [21]. The derivations lead to the iterative procedure described by equation 3 and assume photon emissions that follow Poisson statistics, which is generally accepted to be the case for fluorophores.

$$\hat{f}_i^{(n+1)}=\frac{\hat{f}_i^{(n)}}{\sum_j h_{ji}}\sum_j h_{ji}\frac{g_j}{\sum_m h_{jm}\hat{f}_m^{(n)}} \quad . \qquad 3$$

2) The system matrix for fluorescence OPT

The system matrix $\mathbf{H}$ contains elements h_{ij} which are the probabilities of photons emitted within voxel b i eing detected at pixel j. Because of the optics involved in OPT, the calculation of the h_{ij} can be performed in three steps. The discussion that follows assumes idealised geometric ray optics and ignores the effects of diffraction, which were fully modeled using Fourier Optics in our earlier paper [20]. The reason for this approach is to simplify the computationally intensive calculation of the

system matrix $\mathbf{H}$. The effects of diffraction tend to become less pronounced and more similar to those of geometrical optics away from the focal plane, which is where the vast majority of voxels lie.

First step

Denote by $P_{obj}(i)$ the probability of a photon emitted within voxel i passing through the objective aperture. This is given by

$$P_{obj}(i)=\frac{\Omega_{obj}(i)}{4\pi} \quad , \qquad 4$$

where $\Omega_{obj}(i)$ is the solid angle described by the point at the centre of voxel i nd the objective aperture; a quantity easy to calculate using geometry.

Second step

Denote by $P_{pix}(j,i)$ the probability of a photon emitted within voxel i which has passed through the objective aperture, arriving at pixel j. This probability is given by

$$P_{pix}(j,i)=\frac{\Omega(j,i)}{\Omega_{obj}(i)} \qquad 5$$

where $\Omega(j,i)$ is the solid angle described by the voxel i and the pixel j on a virtual CCD detector at the focal plane. Introducing a virtual CCD detector at the focal plane of the system allows us to ignore the effects of magnification, the pixel size of the virtual detector being easily determined both experimentally and analytically.

Third step

The probability of a photon emitted within voxel i, passing through the objective aperture, and arriving at pixel j is given by the product of equations 4 and 5, and thus

$$h_{ij}=\frac{\Omega(j,i)}{4\pi} \quad . \qquad 6$$

3) Fit between the model and the measured data

Using a system matrix calculated according to the methods described in the previous section, several OPT images were calculated using the relation $\mathbf{g}=\mathbf{Hf}$ for a point source at the positions used for the measurement of the impulse response of the system, described in section 2.2. The maximum values of each simulated image are plotted against defocus in figure 4, along with the measured values from figure 1.

The fit between the simulated data and the measured data, whilst not perfect, is reasonably close. A better fit can be obtained by accounting for the effects of diffraction, as in [20], but for the purposes of calculating the system matrix in reasonable time, the simple geometric optics model has been adopted.

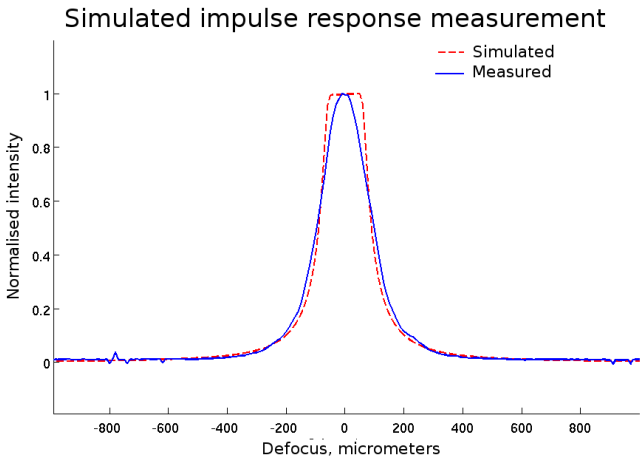

Figure 4. The results of simulating the impulse response measurement described in section 2.2 with the geometrical optics model of image formation described above.

III. RESULTS

A digital computer phantom was created using a 100x100x10 grid voxels, three groups of which were assigned an intensity of 100. The groups were limited to regions of slice 5 and were each 11x11x1 voxels in size. See figure 5. The size of the phantom was chosen so as to fill the field of view of an assumed 2.5x objective with an iris used to reduce the numerical aperture of the system to around 60% of the full numerical aperture.

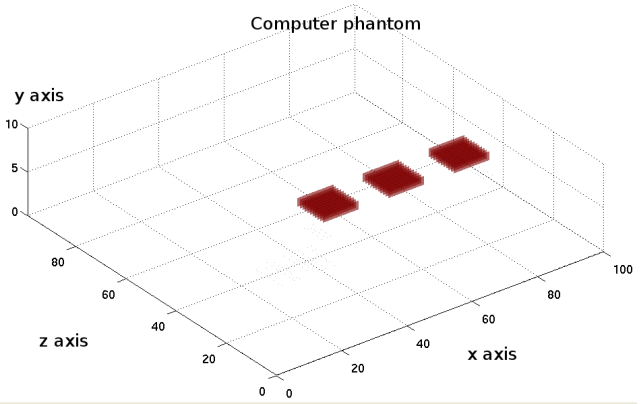

Figure 5. The digital fluorescence OPT phantom consists of a grid of voxels all of zero fluorescence intensity except for three groups of voxels on slice 5 of intensity 100.

100 equally spaced fluorescence OPT projections were calculated over 2π radians using the digital phantom as a sample. Poisson photon emission was assumed and the relation $\mathbf{g}=\mathbf{Hf}$ was used to calculate the projections. Blurring results in slices 3, 4, 6 and 7 receiving fluorescence contribution from the fluorescent material in slice 5. See figure 6.

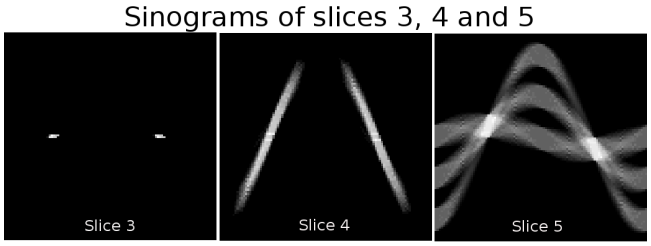

Figure 6. Sinograms of slices 3, 4 and 5. Note the contribution of the fluorescence in slice 5 to slices 3 and 4 in some projections (also slices 6 and 7, not shown) due to blurring.

A. Qualitative comparison of individual reconstructed slices

Reconstructions of the digital phantom were performed using the slice by slice FBP algorithm and the 3D MLEM algorithm. Slices 3, 4, 5, 6 and 7 were assigned non-zero values in all reconstructions. Slices 6 and 7 were identical with slices 4 and 3, due to symmetry. The FBP algorithm resulted in considerable streak artifact and fluorescence being assigned to slices 3, 4, 6 and 7, despite the original digital phantom only expressing fluorescence in slice 5. See figure 7.

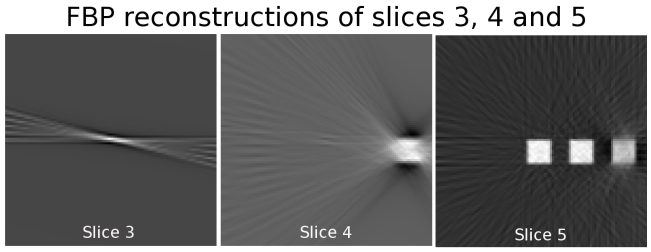

Figure 7. FBP reconstructions of slices 3, 4 and 5 of the digital phantom. Slices 3 and 4 show considerable fluorescence despite zero fluorescence in the digital phantom in these slices. The intensities in slice 5 are reduced towards the edge of the image. All slices suffer from streak artifact, which is associated with the FBP algorithm.

After 50 iterations, the MLEM algorithm performed considerably better than FBP, assigning very low fluorescence intensities in slices other than 5 and very high contrast fluorescence in slice 5 with no streak artifact and a very high signal to noise ratio. See figure 8.

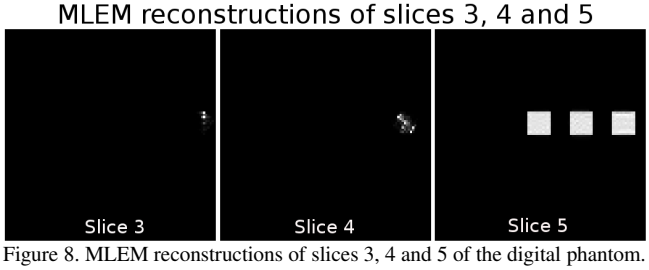

Figure 8. MLEM reconstructions of slices 3, 4 and 5 of the digital phantom. Slices 3 and 4 show very small contributions despite zero fluorescence in the digital phantom in these slices. The intensities in slice 5 appear equal. None of the slices suffer from streak artifacts.

B. Quantitative comparison of slice 5

A *quantitative* comparison of the FBP and MLEM reconstructions of slice 5 illustrates the *quantitative* shortcomings of the FBP algorithm when applied to fluorescence OPT.

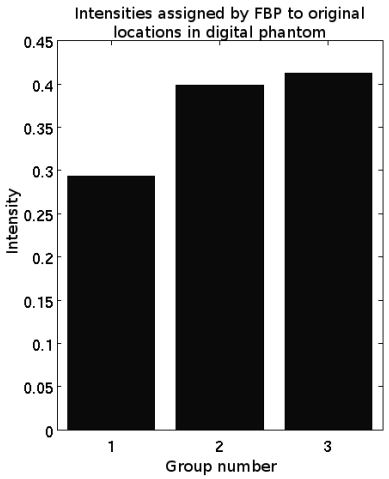

Figure 9. Intensities assigned by the FBP algorithm to the original regions of fluorescence in the digital phantom, group 1 being the outermost group, group 3 being the innermost group and group 2 being the the group midway between groups 1 and 3. The intensities towards the edge of the reconstruction of slice 5 are reduced. All intensities are assigned a significantly lower value than the original value of 100 in the digital phantom.

The intensities assigned by the FBP algorithm to the three groups of fluorophores in slice 5 vary noticeably with their distance from the centre of rotation whilst the intensities of the same groups in the MLEM reconstruction remain constant. See figures 9 and 10.

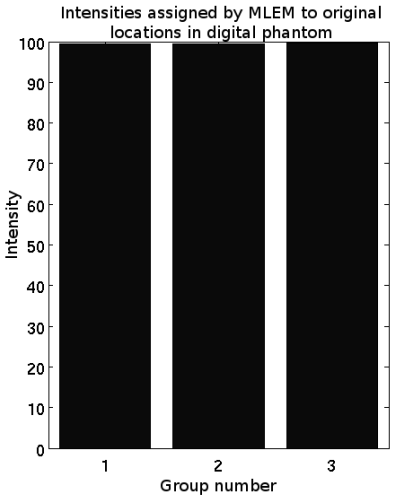

Figure 10. Intensities assigned by the MLEM algorithm to the original regions of fluorescence in the digital phantom, group 1 being the outermost group, group 3 being the innermost group and group 2 being the the group midway between groups 1 and 3. The intensities all appear to have the correct value of 100.

C. Comparison of 3D rendered reconstructions

The three dimensionally rendered FBP reconstruction of the digital phantom reveals both the *quantitative* and the *qualitative* drawbacks of using the FBP algorithm for fluorescence OPT reconstruction. Both the intensity and the signal to noise ratio of the FBP reconstruction are dependent upon distance from the axis of sample rotation. See figure 11.

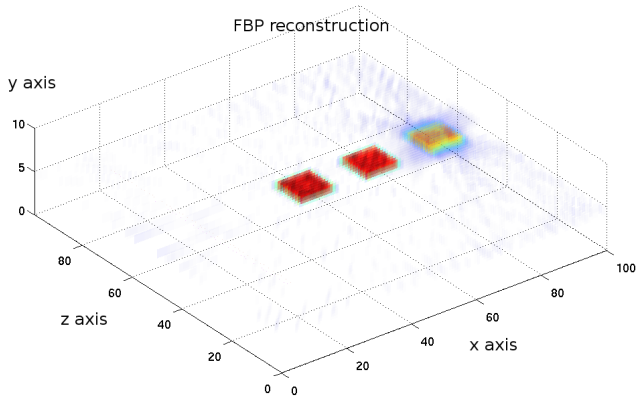

Figure 11. Rendering of an FBP reconstruction of the digital phantom. Note the reduced intensity and lower resolution towards the edge of the volume.

The three dimensionally rendered MLEM reconstructions of the digital phantom show that the reconstruction is *quantitatively* correct and *qualitatively* superior to the FBP reconstruction. See figure 12.

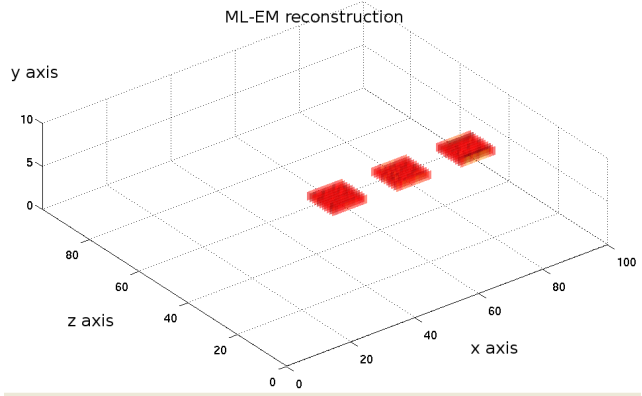

Figure 12. Rendering of a MLEM reconstruction of the digital phantom. Note the high resolution and approximately constant intensity of fluorescence throughout the volume.

IV. CONCLUSIONS

The standard FBP algorithm has been shown to produce *quantitatively* unreliable images that also suffer from *qualitative* drawbacks such as blurring and streak artifact when applied to fluorescence OPT data. Using a model of image formation for fluorescence OPT, the MLEM algorithm has been shown to produce reconstructions that are both *quantitatively* correct and *qualitatively* superior to those produced using the FBP algorithm. This method of reconstruction accounts for the physics of blur and isotropic photon emission by fluorophores.

We are currently working on incorporating the full diffraction based model of image formation into the system model. Once this complete system model is operational, the MLEM algorithm should provide a means of modeling higher numerical apertures in OPT experiments. In this way, the MLEM algorithm may allow a higher signal to noise ratio to be obtained in OPT projections and thus OPT reconstructions.

REFERENCES

[1] J. Sharpe et al., "Optical Projection Tomography as a Tool for 3D Microscopy and Gene Expression Studies," *Science*, vol. 296, Apr. 2002, pp. 541-545.

[2] A. Asayesh et al., "Spleen versus pancreas: strict control of organ interrelationship revealed by analyses of Bapx1-/- mice," *Genes Dev.*, vol. 20, Aug. 2006, pp. 2208-2213.

[3] M. Oldham et al., "Three-dimensional imaging of whole rodent organs using optical computed and emission tomography," *Journal of Biomedical Optics*, vol. 12, Jan. 2007, pp. 014009-10.

[4] J. Kerwin et al., "3 dimensional modelling of early human brain development using optical projection tomography," *BMC Neuroscience*, vol. 5, 2004, p. 27.

[5] K. Lee et al., "Visualizing Plant Development and Gene Expression in Three Dimensions Using Optical Projection Tomography," *Plant Cell*, vol. 18, Sep. 2006, pp. 2145-2156.

[6] M. Fauver et al., "Three-dimensional imaging of single isolated cell nuclei using optical projection tomography," *Optics Express*, vol. 13, May. 2005, pp. 4210-4223.

[7] M. Oldham et al., "Three-dimensional imaging of xenograft tumors using optical computed and emission tomography," *Medical Physics*, vol. 33, 2006, pp. 3193-3202.

[8] C.G. Arques et al., "Cell tracing reveals a dorsoventral lineage restriction plane in the mouse limb bud mesenchyme," *Development*, vol. 134, Oct. 2007, pp. 3713-3722.

[9] L. McGurk et al., "Three-Dimensional Imaging of Drosophila melanogaster," *PLoS ONE*, vol. 2, 2007; http://www.pubmedcentral.nih.gov/articlerender.fcgi?artid=1952176.

[10] R.J. Bryson-Richardson and P.D. Currie, "Optical projection tomography for spatio-temporal analysis in the zebrafish," *Methods in Cell Biology*, vol. 76, 2004, pp. 37-50.

[11] R.J. Bryson-Richardson et al., "FishNet: an online database of zebrafish anatomy," *BMC Biology*, vol. 5, 2007; http://www.pubmedcentral.nih.gov/articlerender.fcgi?artid=2031877.

[12] J. Sharpe, "Optical Projection Tomography as a New Tool for Studying Embryo Anatomy," *Journal of Anatomy*, vol. 202, Feb. 2003, pp. 175-181.

[13] H. Sato et al., "Optical Projection Tomography as a new tool for visualising gene expression," *Reproductive Toxicology*, vol. 24, Jul. 2007, p. 66.

[14] M.J. Boot et al., "In vitro whole-organ imaging: 4D quantification of growing mouse limb buds," *Nat Meth*, vol. 5, Jul. 2008, pp. 609-612.

[15] E. Truernit et al., "High-Resolution Whole-Mount Imaging of Three-Dimensional Tissue Organization and Gene Expression Enables the Study of Phloem Development and Structure in Arabidopsis," *Plant Cell*, Jun. 2008, p. tpc.107.056069.

[16] M.K. Hajihosseini et al., "Localization and fate of Fgf10-expressing cells in the adult mouse brain implicate Fgf10 in control of neurogenesis," *Molecular and Cellular Neuroscience*, vol. 37, Apr. 2008, pp. 857-868.

[17] H. Sato et al., "Visualizing expression patterns of Shh and Foxf1 genes in the foregut and lung buds by optical projection tomography," *Pediatric Surgery International*, vol. 24, Jan. 2008, pp. 3-11.

[18] Y. Wang and R. Wang, "Improved image-forming optics for transmission optical projection tomography," *Three-Dimensional and Multidimensional Microscopy: Image Acquisition and Processing XIV*, San Jose, CA, USA: SPIE, 2007, pp. 644304-5; http://link.aip.org/link/?PSI/6443/644304/1.

[19] J.R. Walls et al., "Resolution improvement in emission optical projection tomography," *Physics in Medicine and Biology*, vol. 52, May. 2007, pp. 2775-2790.

[20] A. Darrell et al., "Weighted filtered backprojection for quantitative fluorescence optical projection tomography," *Physics in Medicine and Biology*, vol. 53, 2008, pp. 3863-3881.

[21] L.A. Shepp and Y. Vardi, "Maximum Likelihood Reconstruction for Emission Tomography," Medical Imaging, IEEE Transactions on, vol. 1, 1982, pp. 113-122.